ELSEVIER

Earth and Planetary Science Letters 158 (1998) 67–79

EPSL

$^{40}Ar/^{39}Ar$ thermochronometry of K-feldspar from the KTB borehole, Germany

Andrew C. Warnock *, Peter K. Zeitler

Department of Earth and Environmental Sciences, Lehigh University, Bethlehem, PA 18015, USA

Received 22 July 1997; revised version received 18 December 1997; accepted 2 February 1998

Abstract

The great depth and relatively steep geothermal gradient (~29ºC/km) of the KTB deep crustal borehole, located in the Bavarian region of Germany, provides the basis for our study of diffusive argon loss in K-feldspar. The observed borehole temperature at 9 km is ~265ºC which reaches well into the argon closure interval for K-feldspar (~125–350ºC). Four microcline and two adularia samples distributed relatively evenly down the 9.1-km deep borehole were analyzed by the $^{40}Ar/^{39}Ar$ method. The thermal histories of the shallow samples are consistent with existing thermochronologic data from the borehole. After correction for chlorine correlated excess ^{40}Ar, the deepest two samples result in age spectra that record zero apparent ages over the first few percent of ^{39}Ar released, which is predicted by diffusion theory where a range of diffusion volumes are present. Inverse modeling of the argon kinetics of these two deep samples reveals that the present elevated geothermal gradient in the borehole has existed for only the last approximately one million years. Recent volcanism within 30 km of the borehole is likely the source of this present-day thermal pulse.

Keywords: KTB; K-feldspar; Ar-40/Ar-39; absolute age; dates; thermal history

1. Introduction

$^{40}Ar/^{39}Ar$ dating of K-feldspar has attracted considerable attention over the last decade by offering the promise of recording thermochronometric information over a temperature range of ~350–125ºC. This stems from the presence of multiple argon diffusion domains within K-feldspar. Partial out gassing laboratory experiments and field studies (e.g. [1,2]) show the lowering of the first portion of the age spectrum with little affect on the final portion of the ^{39}Ar released [3]. This behavior is consistent with diffusion from a range of domain sizes rather than a single volume. Since these early studies, much has been learned about the argon systematics in K-feldspar. However, more tests of the temperature calibration are needed. Fission track geochronologists have long relied on shallow boreholes to study track annealing (e.g. [4,5]). The KTB borehole in Germany offers a unique opportunity to observe argon diffusion behavior in K-feldspar because the temperature at the bottom of the hole (~265ºC) reaches well into the closure interval (~125–350ºC) of a typical K-feldspar. A deep sample should, therefore, reflect both open-system behavior in its small domains, and closed-system behavior in its large domains.

* Corresponding author. Fax: +1 (610) 758-3677; E-mail: aw05@lehigh.edu

0012-821X/98/$19.00
PII S0012-821X(98)00044-2

2. Geologic setting

The KTB scientific borehole is located near the town of Windischeschenbach in the northeastern Bavarian region of Germany (Fig. 1). The drill site was originally chosen based primarily on seismic reflection studies that indicated that the core of the deeply eroded Variscan orogen lay beneath a shallow unit called the Zone of Erbendorf–Vohenstrauss (ZEV). Unfortunately, drilling has revealed that the ZEV is far from shallow. In fact, it has been tectonically thickened by a series of reverse faults and spans the entire depth of the borehole [7].

Mica and amphibole K/Ar and $^{40}Ar/^{39}Ar$ data from the borehole show some scatter, but virtually no systematic variation with depth (Fig. 2) [7,9,10]. The amphiboles to a depth of 5 km record cooling through ~500°C at ~375 Ma. Muscovite to a depth of 9 km records cooling through ~350°C at ~365 Ma, and biotite over the same depth range records cooling through ~300°C from ~315 Ma. The lack of large age variations with depth indicates that tectonic thickening occurred while the rocks were below

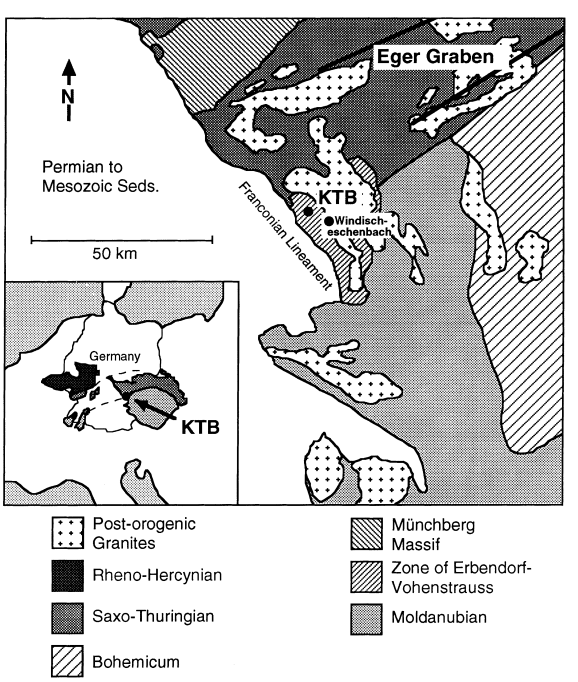

Fig. 1. Generalized geologic map of the KTB borehole region (after Ref. [6]).

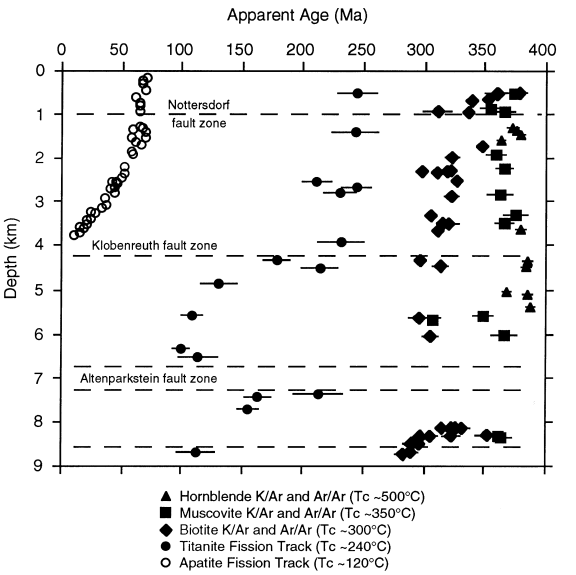

Fig. 2. Apatite and titanite fission track [5,8] and biotite, muscovite, and hornblende K/Ar and $^{40}Ar/^{39}Ar$ [9,10] depth profiles from the KTB borehole. Error bars are 1σ. Note periods of rapid cooling at ~240, 120–95, and 65 Ma.

~300°C, the assumed closure temperature for biotite [7]. The presence of fission tracks in titanite (Fig. 2) and zircon from the bottom of the hole [7] suggests that the deepest rocks in the borehole have not been much hotter than they currently are since the late Paleozoic regional emplacement of postorogenic (Rb–Sr, 320–290 Ma [11]) granitic plutons (Fig. 1).

Deep crustal seismic reflection studies have revealed several prominent steeply dipping reflectors [12]. These reflectors intersect the borehole at shear zones and are interpreted as reverse faults. The most prominent fault is the Altenparkstein fault (7260–6850 m) which outcrops at the surface at the Franconian Lineament (Fig. 1) [13]. The Klobenreuth fault is seen at ~4250 m, and may also outcrop at the surface at or near the Franconian Lineament. Other important faults include the Nottersdorf fault zone at ~500–1500 m [14] and an unnamed fault at 8.7 km [13]. Alluvial fan deposits to the west of the Franconian Lineament record Triassic and Cretaceous uplift events [15,16]. Timing of these events has been more tightly constrained by fission track ages on apatite and titanite from the borehole (Fig. 2) [5,7,8]. Rapid uplift at ~240 Ma has been attributed to N–S compressional wrench tectonics. The com-

pressional effects of the Alpine orogeny are seen at ~120 and 65 Ma. The most recent activity is the extension of the Eger graben to the northeast (Fig. 1) which has been volcanically active since the Late Pliocene–Early Miocene. The most recent eruption was 28 km to the northeast of the borehole and has been dated at ~260 ka [17].

The measured geothermal gradient in the borehole is approximately 28°C/km [18]. However, the natural equilibrium of the region's gradient was depressed as a result of drilling, therefore 29°C/km is probably a closer estimate to the equilibrium geothermal gradient (T. Kohl, pers. comm.).

3. Methods

3.1. Samples

Primary K-feldspar is a difficult mineral to find in the metabasites and paragneisses sampled by the KTB borehole. The majority of the K-feldspar occurs as adularia found in secondary veins. After examining borehole logs and many thin sections, it became apparent that the only way to find primary K-feldspar was by using trial and error. An amount of 300–500 g of core or cuttings were obtained every ~375 m yielding a total of 24 samples. Samples above 7.4 km were taken from cores, while the deeper samples were from cuttings. Prior to pulverizing, cuttings were carefully hand-picked to remove any grains of anomalous lithology, crystal size or degree of rounding. This was done to minimize contamination from higher depths within the borehole. All samples were crushed and sized between 150 and 180 μm. K-feldspar was separated using several passes through sodium polytungstate. Thirteen of the 24 samples contained K-feldspar. Of the 13 K-feldspar-bearing samples, only 6 yielded 99% pure K-feldspar after magnetic separation and final hand-picking. The remaining 7 samples contained both K-feldspar and plagioclase having similar colors and densities. Conveniently, the pure samples were relatively evenly distributed down the hole (0, 2804, 3203, 6149, 7762, and 9000 m). The separates were checked with a cathodoluminescence microscope in order to determine if the feldspar was primary or authigenic. Igneous K-feldspars emit a bright blue luminescence at 10 kV [19]. The low crystallization temperature of authigenic K-feldspar prevents the substitution into the lattice of impure elements which are believed to produce luminescence [20]. Four of the samples luminesced indicating that they have a high-temperature origin (microcline). The two remaining samples (KTB-2804m and KTB-6149m) did not luminesce indicating a low-temperature origin (adularia). The occurrence of the two adularia samples is consistent with these observations: sample KTB-2804m occurs as centimeter-sized crystals of pink adularia in a calcite vein; KTB-6149m occurs in much finer, millimeter-sized veins and is white in color. Chemical compositions of all of the samples were determined using a JEOL 733 electron microprobe. Cation compositions are listed in Table 1.

Table 1
Electron microprobe results

Sample	Orthoclase	Albite	Anorthite	*n*
KTB-0m	93.9	5.5	0.6	4
KTB-2804m	97.1	2.8	0.1	3
KTB-3203m	97.1	2.8	0.1	3
KTB-6149m	93.8	4.4	1.8	3
KTB-7762m	97.8	2.2	0.0	2
KTB-9000m	93.5	6.4	0.1	4

3.2. Sample irradiation

Samples (3–26 mg) were enclosed in tin packets and sealed under vacuum in quartz glass vials for irradiation in the L67 position at the University of Michigan Ford reactor. Samples KTB-2804m, KTB-3203m, KTB-6149m, KTB-7762m, and KTB-9000m were irradiated for 40 h and KTB-0m was irradiated for 20 h. The long durations of the irradiations were chosen to optimize the abundance of ^{38}Ar derived from the neutron interaction with chlorine to facilitate the chlorine correction for excess argon discussed below. Biotite standard GA1550 [21] was used to monitor the fast neutron flux. CaF_2 and K_2SO_4 were used to quantify interfering reactions on calcium and potassium.

3.3. Argon analyses

Argon gas was extracted from the samples in a double-vacuum resistance furnace [22]. The sam-

ples were heated in a clean crucible (tantalum lined with molybdenum) with temperature control precise and accurate to 0.5%. The gas released on heating was subsequently cleaned to remove active gases using two SAES GP-50 titanium getters, one operated at 400ºC and the other at room temperature. Temperature-dependent extraction line blanks were well characterized, atmospheric in composition, and never more than 10% of the ^{40}Ar beam. Argon analyses were carried out statically on a VG 3600 mass spectrometer equipped with an electron multiplier collector with an effective sensitivity of 4×10^{-17} mol/mV. Corrections for mass discrimination, decay of ^{37}Ar and ^{39}Ar, interfering reactions on calcium and potassium during irradiation, and extraction line blanks were applied to the data. Standard decay constants and isotopic abundances were used [23]. All uncertainties are reported as 1σ.

Step-heating experiments were conducted using the isothermal-duplicate approach [24]. The isothermal-duplicate step-heating method is used to identify a component of excess (non-radiogenic) argon that is sited in fluid inclusions and is correlated with chlorine ($^{40}Ar_E$/Cl). The first step of the isothermal pair will cause fluid inclusions to decrepitate as well as release gas from the crystal's lattice. Because the decrepitation of fluid inclusions is strongly temperature-dependent, the second step at the same temperature releases gas that is dominantly from the lattice. The correlation between the change in $^{40}Ar^*$/K and the change in Cl/K from several isothermal pairs represents the excess ^{40}Ar component correlated with chlorine-derived ^{38}Ar. This component can be subtracted from the affected portion of the age spectrum.

3.4. Modeling of age spectra

Deriving time–temperature histories from K-feldspar data is relatively straightforward in the case of samples that have only experienced cooling. Under such circumstances, a unique solution is possible. However, in the case of episodic loss, a unique solution is not possible. The recent advent of inversion schemes has allowed exploration of the range in thermal histories that produce the observed age spectra [25,26]. The best estimate of the actual thermal history is defined by using available geologic constraints to narrow down the range in possible thermal histories.

All of the microcline samples studied here have been evaluated using a model [25] which uses the controlled-random-search algorithm to find thermal histories that when fed into a finite-difference diffusion model produce age spectra that match the observed spectra. Samples KTB-0m and KTB-3203m were each modeled assuming cooling only. Samples KTB-7762m and KTB-9000m have been modeled allowing cooling and heating. The reason for this is discussed below. Samples KTB-9000m and KTB-7762m were also modeled with a forward model [27] for comparison.

4. Results

4.1. Chlorine correlated excess argon

Chlorine correlations were achieved over a rather narrow temperature range of 550–750ºC and are consequently defined by 3–4 points (e.g., Fig. 3a). $^{40}Ar_E$/Cl ratios ranged from 3.6×10^{-5} to 4.3×10^{-4}. Samples KTB-0m and KTB-3203m did not contain enough excess argon to produce a satisfactory correlation. Sample KTB-7762m shows an apparent correlation, however, because the correlation line narrowly misses the origin, due to an insufficient number of data points between 550 and 750ºC to define the exact correlation, it must be viewed as an approximation. Sample KTB-2804m did not have a component of excess argon.

4.2. Age spectra

Results of ^{40}Ar/^{39}Ar analyses are summarized in Figs. 3–8 (see also **EPSL Online Background Dataset** [1]). Data for sample KTB-9000m are listed in Table 2. Isothermal-duplicate step-heating resulted in oscillating age spectra at low (<800ºC) laboratory temperatures for all samples except KTB-2804m. Fig. 3b, Fig. 4a and Fig. 5a illustrate the dramatic affect of the chlorine correction on the age spectra. Most notable is that sample KTB-9000m (Fig. 3b) shows a zero age for the first approximately 7% of ^{39}Ar released after correction for excess argon. The

[1] http://www.elsevier.nl/locate/epsl,
mirrorsite: http://www.elsevier.com/locate/epsl.

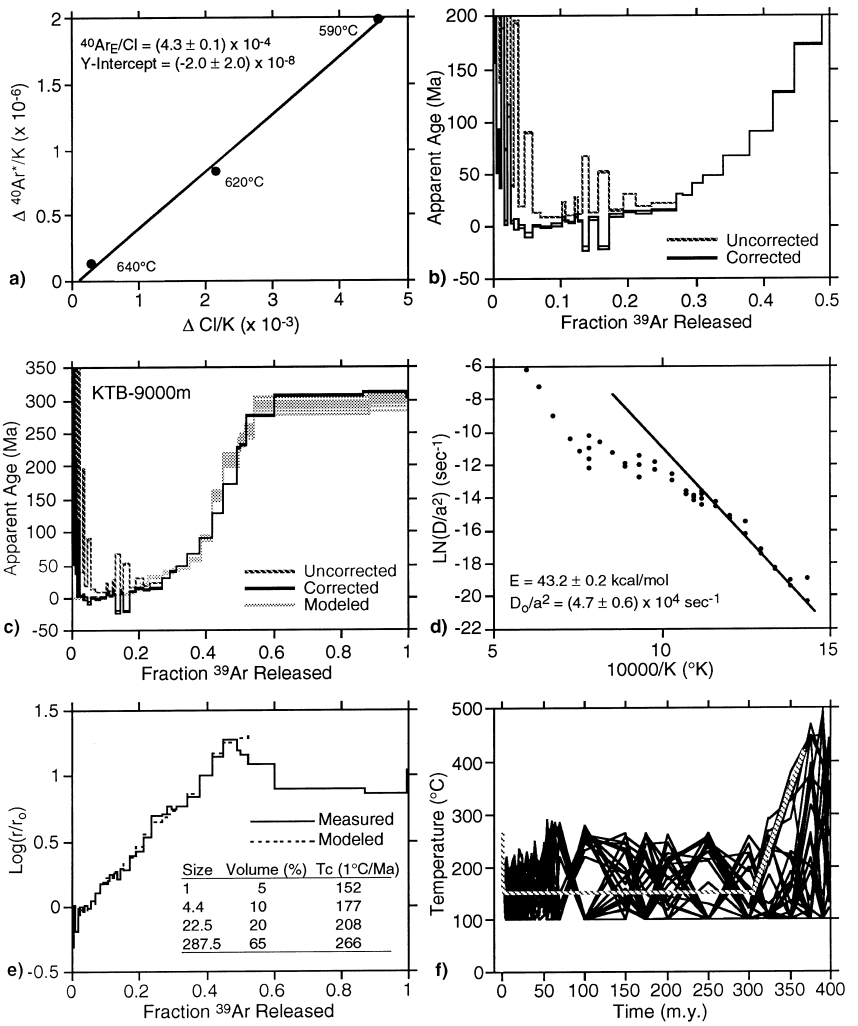

Fig. 3. $^{40}Ar/^{39}Ar$ results from microcline sample KTB-9000m. In situ equilibrium temperature ~265°C. (a) Chlorine-correlation plot. (b) Detail of the first ~7% of ^{39}Ar released showing zero age after correction for chlorine-correlated excess argon. (c) Uncorrected, corrected, and modeled age spectra. (d) Arrhenius plot showing linear regression lines used to calculate the activation energy and diffusion coefficient. (e) Log(r/r_o) plot of both the measured spectrum and the modeled domain structure. (f) Plot of 25 thermal histories generated from model allowing both cooling and heating. The forward model is plotted in gray.

chlorine correction resulted in a slight over correction in sample KTB-7762m thus yielding negative ages (Fig. 4a). This is attributed to the fact that the chlorine correlation did not intercept the origin. It is inferred that the first 5% of ^{39}Ar released records a zero age, based on the concave-down morphology of the spectrum between 15 and 5% ^{39}Ar released. Samples KTB-6149m and KTB-2804m have age spectra morphologies that are different from the other K-feldspar spectra from the KTB (Fig. 5a and Fig. 7a). The first 20% of ^{39}Ar released show a concave-down shape.

KTB-3203m shows a hump at ~20% ^{39}Ar released (Fig. 6a). Hump shaped age spectra in K-feldspars are not completely understood. One explanation is that the decreasing ages after the hump are an artifact of the onset of melting. The sharp lengthening of the diffusion path (drop) seen on the log(r/r_o) plot (Fig. 6c) is interpreted to be due to the homogenization of diffusion domains. Because

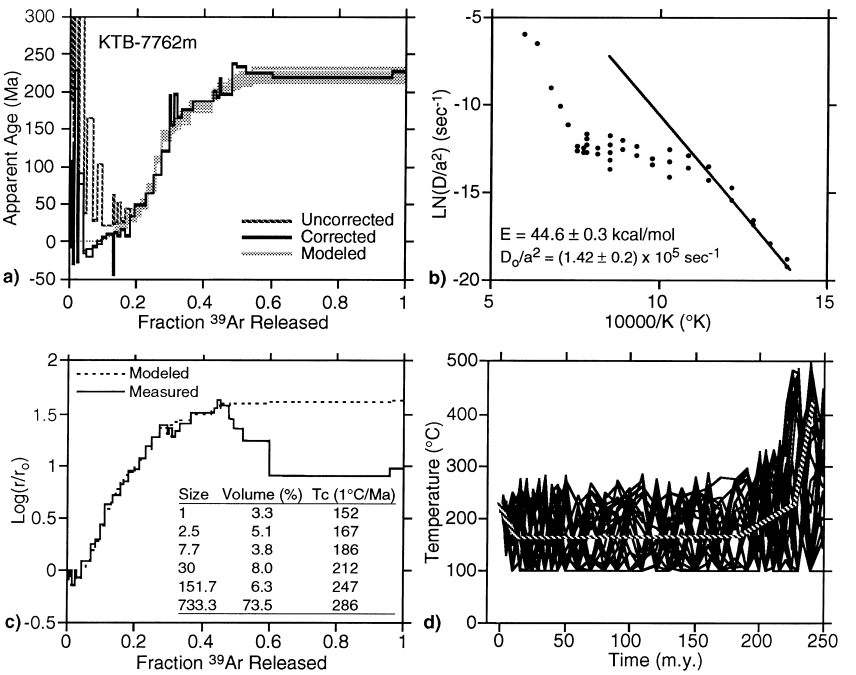

Fig. 4. $^{40}Ar/^{39}Ar$ results from microcline sample KTB-7762m. In situ equilibrium temperature ~228°C. (a) Uncorrected, corrected ($^{40}Ar_E/^{38}Ar_{Cl} = 693 \pm 15$, $Y-$intercept $= -0.7 \pm 0.2$), and modeled age spectra. (b) Arrhenius plot. (c) $\mathrm{Log}(r/r_o)$ plot. (d) The forward model is plotted in gray.

the hump in the age spectrum corresponds to the drop on the $\log(r/r_o)$ plot, we believe that the two phenomena are related. The surface sample (Fig. 8a) also shows a hump, except to a lesser degree. The second steps from the isothermal pairs from both KTB-3203m and KTB-0m were taken as the best estimate of the apparent age in the absence of statistically significant chlorine correction. None of the samples appear to have anion-sited excess argon which typically causes ages to increase dramatically in the last few percent of ^{39}Ar released [28,29].

4.3. Diffusion domain analysis

Arrhenius data shown in Figs. 3–8 are typical of slowly cooled K-feldspar. Reference diffusion parameters ranged from $E = 39.4$ kcal/mol and

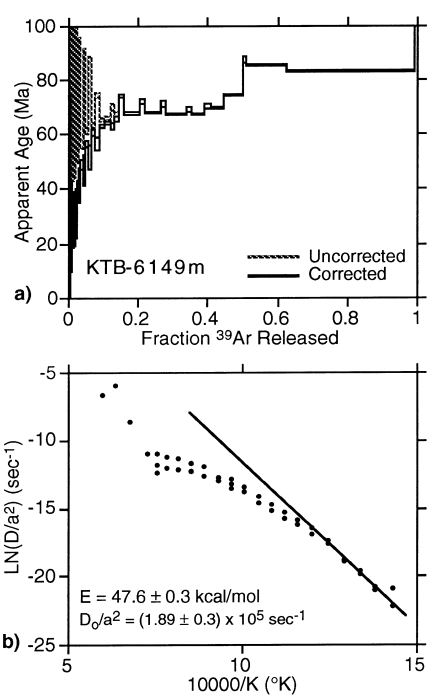

Fig. 5. $^{40}Ar/^{39}Ar$ results from adularia sample KTB-6149m. In situ equilibrium temperature ~181°C. (a) Uncorrected and corrected ($^{40}Ar_E/^{38}Ar_{Cl} = 83 \pm 10$, $Y-$intercept $= -0.8 \pm 0.4$) age spectra. (b) Arrhenius plot.

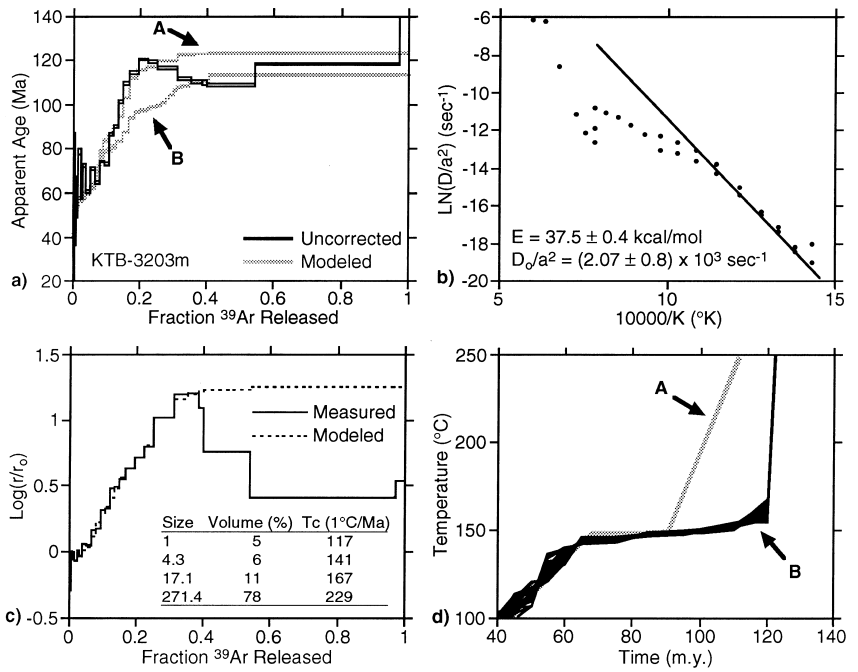

Fig. 6. $^{40}Ar/^{39}Ar$ results from microcline sample KTB-3203m. In situ equilibrium temperature ~94°C. (a) Uncorrected and modeled age spectra. Modeled spectrum *A* assumes that the decreasing ages following the hump are an artifact of the onset of melting. Spectrum *B* assumes that the hump is the artifact. (b) Arrhenius plot. (c) $\mathrm{Log}(r/r_o)$ plot. (d) End member thermal histories indicating that initial cooling occurred between ~120 and 95 Ma. Final cooling took place at ~65 Ma.

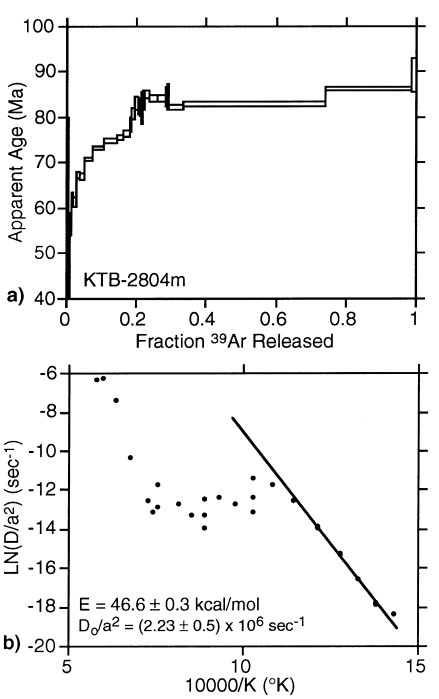

$D_o/a^2 = 5.39 \times 10^4\ s^{-1}$ to $E = 47.6$ kcal/mol and $D_o/a^2 = 1.89 \times 10^5\ s^{-1}$. The departure from linearity at high temperatures has been shown to represent the effect of a range of diffusion domain volumes [1,27, 30]. Dependence of Arrhenius data on the laboratory heating schedule can be removed by constructing a $\log(r/r_o)$ plot (Figs. 3–8) [31]. Forward modeling of the $\log(r/r_o)$ data assuming an infinite slab diffusion geometry allows the determination of relative size, volume, and closure temperatures for the domains present.

The microcline samples have between 4 and 6 domains with closure temperatures ranging from ~115 to ~286°C for a cooling rate of 1°C/Ma. As is typical, the age spectra resemble the $\log(r/r_o)$ spectra due to the genetic relationship between ages and diffusion domains.

Fig. 7. $^{40}Ar/^{39}Ar$ results from adularia sample KTB-2804m. In situ equilibrium temperature ~82°C. (a) Age spectrum. (b) Arrhenius plot.

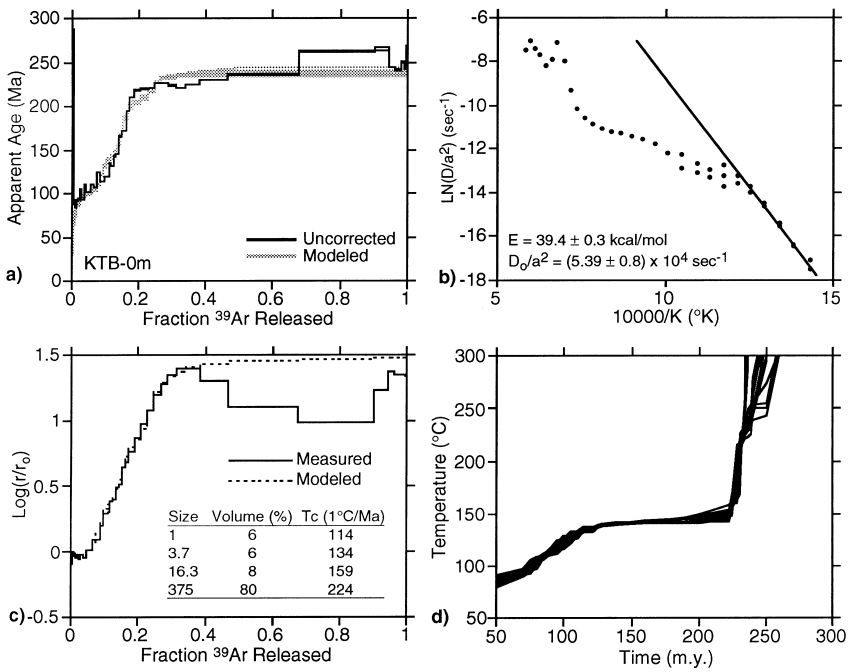

Fig. 8. $^{40}Ar/^{39}Ar$ results from microcline sample KTB-0m. (a) Uncorrected and modeled age spectra. (b) Arrhenius plot. (c) $Log(r/r_o)$ plot. (d) Thermal history.

4.4. Modeled thermal histories

Sample KTB-0m shows rapid cooling events at ~230 and 120 Ma (Fig. 8d). Due to the uncertain nature of the hump in the age spectrum of sample KTB-3203m, two end-member models were used to bracket the thermal history (Fig. 6a,d). Fast cooling occurred between ~120 and 95 Ma and then again at ~65 Ma (Fig. 6d). The two deep samples cannot be modeled with the simple cooling approach given the current in situ temperatures of the samples. Allowing the inversion model to use thermal histories that have cooling and heating within geologically reasonable limits yields a population of thermal histories that oscillate (Fig. 3f and Fig. 4d). The oscillating thermal histories in these two samples are an artifact of the model and the fact that domains are incapable of recording information between initial cooling and a thermal pulse. Forward modeling of samples KTB-9000m and KTB-7762m confirms that the observed age spectra can indeed result from a thermal history with initial cooling through the closure interval, a long isothermal segment, and a present-day thermal pulse (Fig. 3f and Fig. 4d).

5. Discussion

5.1. Post-Variscan thermal history

The existing thermochronologic data have been used to constrain the structural history of the borehole region [7]. Each sample studied here comes from a separate fault-bounded section of the borehole, and can be compared with the existing data from the individual blocks. Fig. 9 is a schematic diagram summarizing the time–temperature paths for each of the major fault-bounded blocks constrained by the available apatite [5] and titanite [8] fission track data and supplemented with the K-feldspar data presented here. No attempt has been made to quantitatively reconstruct the spatial path of the blocks or consequently, the isotherms. Spatial relationships implied by the size of the individual blocks and the available time–temperature data assuming a uniform geothermal gradient, however, provide a first order approximation of the structural history.

Sample KTB-9000m passed through 265°C at 313 Ma, most likely in response to regional cooling after emplacement of the nearby postorogenic plutons

Table 2
$^{40}Ar/^{39}Ar$ analytical results for sample KTB-9000m

Temp. (°C)	Dur. (min)	40/39	± (%)	38/39	± (%)	37/39	± (%)	36/39	± (%)	^{39}Ar (mol)	± (%)	Fraction ^{39}Ar	40^* (%)	$40^*/^{39}K$	Age (Ma)	± (Ma)	Corr. age (Ma)	± (Ma)
425	10	582.39	0.5	0.1670	1.1	0.0801	3.8	0.27944	1.4	9.91e−15	0.4	0.002	85.8	499.830	2566.10	8.57	2263.36	12.00
425	20	90.45	0.5	0.0560	1.1	0.0472	2.4	0.14008	1.5	2.80e−15	0.5	0.003	53.8	49.038	485.42	5.70	325.05	9.41
450	10	93.52	0.5	0.0670	1.2	0.0404	3.6	0.14217	1.4	3.00e−15	0.4	0.003	54.7	51.492	506.59	5.48	247.06	11.32
450	20	78.58	0.4	0.0573	0.9	0.0329	1.4	0.16547	1.3	4.21e−15	0.4	0.004	37.5	29.667	308.94	6.28	166.40	9.57
475	10	94.45	0.4	0.0776	0.8	0.0271	5.9	0.09368	1.4	4.56e−15	0.4	0.005	70.4	66.751	632.94	4.21	204.27	12.18
475	20	29.85	0.4	0.0334	0.9	0.0245	1.5	0.03123	1.5	6.53e−15	0.3	0.007	68.4	20.601	220.01	1.80	55.81	4.91
500	10	98.21	0.3	0.1029	0.7	0.0209	2.9	0.01260	1.9	9.16e−15	0.3	0.008	96.0	94.460	841.96	3.36	72.95	20.13
500	20	14.31	0.4	0.0221	0.8	0.0215	1.4	0.00526	2.9	1.06e−14	0.3	0.011	87.9	12.735	139.14	0.89	39.63	2.88
530	10	74.54	0.3	0.0678	0.7	0.0215	2.7	0.00397	3.0	2.68e−14	0.3	0.016	98.3	73.344	684.92	2.78	200.15	11.87
530	20	7.30	0.4	0.0186	0.8	0.0251	1.1	0.00204	4.1	1.80e−14	0.3	0.020	90.1	6.677	74.29	0.50	3.15	2.21
560	10	35.29	0.3	0.0370	0.8	0.0288	1.8	0.00158	5.2	2.36e−14	0.3	0.025	98.4	34.803	357.44	1.59	111.31	5.89
560	20	4.07	0.4	0.0153	0.7	0.0356	1.0	0.00202	2.8	2.91e−14	0.3	0.031	83.4	3.448	38.75	0.30	3.78	1.45
590	10	18.41	0.3	0.0301	0.7	0.0393	1.2	0.00102	5.6	3.47e−14	0.3	0.038	97.9	18.091	194.60	0.92	2.23	4.55
590	20	1.85	0.6	0.0136	0.7	0.0395	1.0	0.00048	6.9	4.39e−14	0.3	0.047	88.9	1.688	19.07	0.17	−0.28	1.16
620	10	8.29	0.3	0.0208	0.7	0.0397	1.1	0.00050	7.0	4.63e−14	0.3	0.057	97.4	8.122	89.98	0.45	−7.58	2.54
620	20	1.32	0.6	0.0130	0.7	0.0360	1.1	0.00038	6.4	5.92e−14	0.3	0.069	87.4	1.186	13.42	0.13	0.89	1.08
620	40	0.91	0.7	0.0127	0.7	0.0300	1.0	0.00039	5.2	7.38e−14	0.3	0.085	82.3	0.774	8.77	0.10	−0.66	1.03
620	80	0.92	0.6	0.0125	0.7	0.0249	1.0	0.00042	4.3	8.72e−14	0.3	0.103	81.7	0.770	8.73	0.09	1.31	0.99
640	10	2.17	1.1	0.0133	1.0	0.0243	2.5	0.00022	50.9	1.68e−14	0.3	0.106	90.9	2.087	23.55	0.47	7.10	1.59
640	20	1.04	1.4	0.0123	0.8	0.0229	1.1	0.00032	15.8	2.84e−14	0.3	0.112	82.9	0.920	10.42	0.24	5.28	1.12
640	40	1.07	0.9	0.0124	0.7	0.0228	1.1	0.00037	8.9	4.41e−14	0.3	0.121	83.8	0.934	10.58	0.16	4.08	1.06
660	10	2.60	0.9	0.0134	0.9	0.0232	1.2	0.00044	17.0	1.90e−14	0.3	0.125	90.4	2.449	27.61	0.37	10.92	1.39
660	20	1.14	1.2	0.0124	0.8	0.0242	1.2	0.00028	16.3	3.06e−14	0.3	0.132	85.6	1.036	11.73	0.22	5.06	1.14
700	10	6.18	0.3	0.0198	0.7	0.0280	1.1	0.00041	7.9	4.69e−14	0.3	0.142	96.9	6.034	67.27	0.35	−21.07	2.31
700	20	1.22	0.6	0.0123	0.7	0.0248	1.0	0.00021	11.7	6.11e−14	0.3	0.154	90.3	1.129	12.78	0.13	7.46	1.04
750	10	4.76	0.3	0.0183	0.7	0.0272	1.3	0.00027	7.7	8.54e−14	0.3	0.172	97.3	4.654	52.10	0.26	−20.24	2.01
750	20	1.47	0.4	0.0123	0.7	0.0265	1.0	0.00024	6.9	9.24e−14	0.3	0.191	92.1	1.378	15.58	0.11	10.16	0.97
800	10	2.84	0.3	0.0134	0.8	0.0325	1.1	0.00021	8.7	9.82e−14	0.3	0.212	96.2	2.759	31.07	0.17	14.05	1.20
800	20	1.75	0.4	0.0123	0.7	0.0314	1.0	0.00020	7.5	1.05e−13	0.3	0.233	94.2	1.670	18.86	0.11	13.29	0.99
800	80	2.09	0.3	0.0125	0.7	0.0301	1.0	0.00025	4.3	1.74e−13	0.3	0.270	94.7	1.990	22.46	0.12	15.73	1.02
850	10	2.75	0.5	0.0128	0.9	0.0331	1.2	0.00010	36.5	4.68e−14	0.3	0.279	96.3	2.689	30.39	0.22		
850	20	2.70	0.4	0.0125	0.7	0.0308	1.0	0.00020	11.9	6.95e−14	0.3	0.294	95.8	2.614	29.45	0.18		
900	10	3.72	0.3	0.0136	0.7	0.0363	1.2	0.00022	9.2	8.14e−14	0.3	0.311	96.8	3.632	40.79	0.21		
950	10	4.43	0.3	0.0137	0.7	0.0358	1.1	0.00018	7.7	1.44e−13	0.3	0.341	97.9	4.352	48.76	0.24		
1000	10	6.09	0.3	0.0141	0.7	0.0275	1.1	0.00016	9.1	1.87e−13	0.3	0.380	98.6	6.019	67.10	0.32		
1000	20	8.29	0.3	0.0146	0.7	0.0179	1.1	0.00020	6.8	1.66e−13	0.3	0.415	98.8	8.210	90.92	0.43		
1000	40	11.83	0.3	0.0158	0.7	0.0163	1.3	0.00031	6.3	1.58e−13	0.3	0.447	98.9	11.711	128.35	0.60		
1000	100	16.14	0.3	0.0169	0.7	0.0153	1.6	0.00044	3.3	1.98e−13	0.3	0.489	99.0	15.983	172.98	0.80		
1050	10	21.40	0.3	0.0188	0.8	0.0217	1.3	0.00025	19.0	5.13e−14	0.3	0.499	99.3	21.297	227.00	1.04		
1100	10	21.97	0.3	0.0194	0.7	0.0293	1.2	0.00054	4.9	1.02e−13	0.3	0.521	99.0	21.782	231.86	1.07		
1200	10	26.50	0.3	0.0247	0.7	0.0340	1.2	0.00058	5.9	3.86e−13	0.3	0.601	99.2	26.306	276.48	1.24		
1300	10	29.63	0.3	0.0212	0.7	0.0150	1.6	0.00055	5.9	1.28e−12	0.3	0.867	99.4	29.444	306.81	1.38		
1400	10	30.23	0.3	0.0157	0.7	0.0219	1.5	0.00047	6.0	6.06e−13	0.3	0.993	99.4	30.062	312.72	1.40		
1450	10	29.54	0.3	0.0178	1.0	0.0361	1.3	0.00037	22.4	3.12e−14	0.3	1.000	99.2	29.404	306.42	1.40		

$J = (6.29 \pm 0.02) \times 10^{-3}$; $(^{36}Ar/^{37}Ar)_{Ca} = (2.072 \pm 0.005) \times 10^{-4}$; $(^{39}Ar/^{37}Ar)_{Ca} = (7.37 \pm 0.05) \times 10^{-4}$; $(^{40}Ar/^{39}Ar)_K = (2.48 \pm 0.09) \times 10^{-2}$; $(^{38}Ar/^{39}Ar)_K = (1.180 \pm 0.001) \times 10^{-2}$; $^{39}Ar_K/K = 1.21 \times 10^{-7}$; $Cl/^{38}Ar_{Cl} = 0.277$ (from Ref. [24]); mass discrimination = 0.9802 ± 0.01; weight = 26.49 mg.

(Fig. 1). KTB-7762m cooled at ~225 Ma possibly due to thrusting above sample KTB-9000m along the unnamed fault at 8700 m. Roughly contemporaneously, KTB-0m also records a rapid cooling event. Titanite fission track data from samples in the top 4 km of the borehole record rapid cooling between 245 and 210 Ma (Fig. 2) [8]. The top 4-km section, therefore, appears to have moved along the Klobenreuth fault zone during the Triassic.

Samples KTB-0m and KTB-3203m were then quickly cooled between approximately 125-95 Ma (Fig. 9). This cooling is probably a result of the displacement along the Altenparkstein fault zone due to the fact that cooling is also recorded by fission

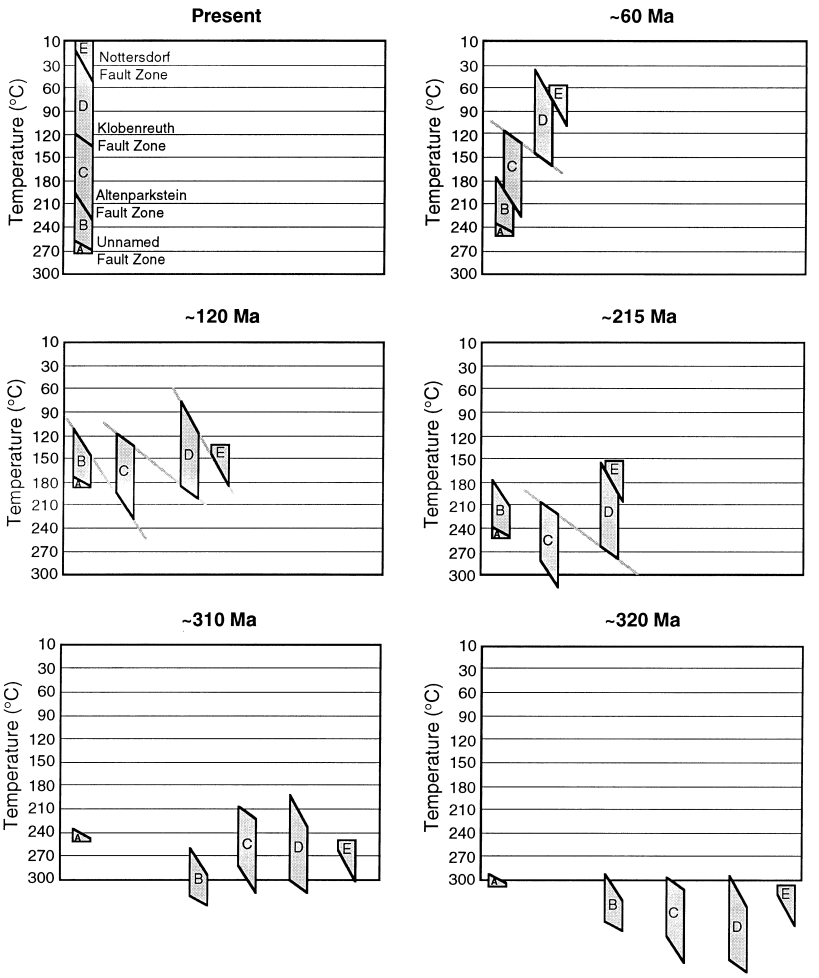

Fig. 9. Schematic summary of the time–temperature paths experienced by the five major blocks that comprise the drilled sequence. Note that the temperature scale is linear and held uniform through time. Depth and distance are not implied.

tracks in titanite (97–129 Ma) sampled at depths of 4.5 to 6.5 km [8] (Fig. 2). A similar faulting event took place between 70 and 60 Ma also along the Altenparkstein fault zone. This event is recorded by sample KTB-3203m as well as apatite fission track ages from the top 2 km (Figs. 2 and 9) [5]. Both the 125–95 and 70–60 Ma events are likely associated with the onset of the Alpine orogeny to the south.

The consistency between the cooling events delineated by the fission track depth profiles and the microclines is strong evidence that the modeled feldspar thermal histories are indeed reliable. Such a comparison is more robust than simply comparing feldspar and fission track data from the surface.

5.2. Significance of zero ages

The top four samples are all currently below their minimum closure temperatures. Samples KTB-7762m and KTB-9000m, however, are at in situ temperatures near the closure temperatures of the largest domains (Fig. 3e and Fig. 4c). It is unlikely that these two samples were kept at precisely these temperatures for up to 300 million years. In addition, KTB-7762m and KTB-9000m cannot be modeled successfully with an isothermal history. There are two alternatives. The first is that the maximum ages recorded by the two bottom samples are not radiogenic in nature. Excess argon trapped in the

large domains (non-chlorine-correlated) during closure would be indistinguishable from radiogenic argon [32]. This hypothesis is not favored because the shallow samples do not appear to be affected, even though they became closed systems under similar geologic conditions and, in the case of KTB-0m and KTB-7762m, contemporaneously. In fact, it has been observed that the sequences 0–560 and 7260–7812 m are also similar in rock association, petrography, and geochemistry [13]. Although the fluid inclusion sited excess argon shows variable $^{40}Ar_E/Cl$ ratios between samples, it will be shown below that the excess argon-bearing fluid inclusions were formed long after the large domains closed.

The preferred scenario is that KTB-9000m and KTB-7762m were uplifted at 313 and 240 Ma, respectively. Uplift continued until Early Cretaceous faulting began to thicken the crust and cause subsidence of samples below the Altenparkstein fault. Modeling of the argon release data from KTB-9000m and KTB-7762m indicates that a present day thermal pulse having a duration on the order of 1 million years is required to explain the observed partially out-gassed small diffusion domains. Quaternary volcanism 28 km to the northeast, associated with the Eger graben, may be the cause of the present-day observed gradient. This short-lived event may also be the cause of the persistence of fission tracks at the bottom of the hole [7].

5.3. Adularia and fluid inclusions

The two adularia samples (KTB-2804m and KTB-6149m) record approximately the same maximum apparent ages, ~85 Ma (Figs. 5 and 7). This implies that a K-rich fluid pulse may have been associated with Alpine-related faulting. Based on the thermal history discussed above, the rocks at these depths were at temperatures high enough (150–250°C) for adularia crystallization. An important observation is that KTB-6149m has a significant component of chlorine-correlated excess ^{40}Ar which appears to be sited in fluid inclusions (Fig. 5a). This suggests that at least some of the fluid inclusions in the KTB borehole are younger than ~85 Ma, the maximum age of KTB-6149m. The presence of chlorine-correlated excess argon bearing fluid inclusions in the lower three samples (KTB-6149m, KTB-7762m, and KTB-9000m) is not surprising. There are three distinct populations of chlorine-bearing fluid inclusions in the KTB borehole: Late Carboniferous aged, low to moderately saline fluid inclusions found in the upper half of the borehole, Cretaceous to recent, moderate to highly saline inclusions increasing in abundance below 6000 m, and recent, low salinity inclusions above 5000 m [33]. The fluid inclusions in the lower three samples, therefore, probably formed no earlier than the Cretaceous. If this scenario is correct, then the excess argon-bearing fluid inclusions were acquired after all of the domains had already closed, and before the small domains were reopened. The formation of excess argon-bearing fluid inclusions, therefore, does not appear to be genetically related to the process of argon closure.

6. Conclusions

Three major conclusions can be drawn from the K-feldspar samples studied here. First, there is good consistency between cooling events delineated by the fission track depth profiles [5,8] and the cooling events recorded by the K-feldspars. This is good evidence that thermal histories derived from K-feldspars are indeed reliable. Second, the bottom two samples record both open- and closed-system behavior as diffusion domain theory predicts. Third, the two deep samples require a short-lived (~1 Ma), present-day thermal pulse to explain the observed zero ages. Recent volcanism in the nearby Eger graben may be the cause of the elevated geotherm and the persistence of titanite and zircon fission tracks [7] at the bottom of the borehole.

Acknowledgements

We would like to thank the KTB program directors and scientists, especially Drs. J. Lauterjung and H.-G. Dietrich for contributing borehole samples and research reports, and Dr. J. Duyster for helpful advice and interesting conversations at the field laboratory. Krista Warnock and David Coyle helped with logistics in Bavaria. Thanks also to Drs. T.M. Harrison, K. Farley, M. Heizler, J. Duyster, and S. Nemming for reviewing the manuscript. This re-

search was supported by Grant EAR-9219595 from the NSF Continental Dynamics Program. *[CL]*

References

[1] P.K. Zeitler, Argon diffusion in partially outgassed alkali feldspar: insights from $^{40}Ar/^{39}Ar$ analysis, Chem. Geol. 65 (1987) 167–181.

[2] F.J. Ryerson, T.M. Harrison, Degassing of argon from microclines within the thermal aureole of the Obsidian Dome conduit, Long Valley Caldera, California: constraints on emplacement history, J. Geophys. Res. 95 (1990) 2781–2792.

[3] A.R. Gillespie, J.C. Huneke, G.J. Wasserburg, An assessment of $^{40}Ar–^{39}Ar$ dating of incompletely degassed xenoliths, J. Geophys. Res. 87 (B11) (1982) 9247–9257.

[4] A.J.W. Gleadow, I.R. Duddy, A natural long-term track annealing experiment for apatite, Nucl. Tracks 5 (1981) 169–174.

[5] D.A. Coyle, G.A. Wagner, E. Hejl, R. Brown, P. Van den haute, The Cretaceous and younger thermal history of the KTB site (Germany): apatite fission-track data from the Vorbohrung, Geol. Rundsch. 86 (1997) 203–209.

[6] U. Schüssler, P. Richter, M. Okrusch, Metabasites from the Oberpfalz target area, Bavaria-Geochemical characteristics and examples of mobile behavior of 'immobile' elements, Tectonophysics 157 (1989) 135–148.

[7] G.A. Wagner, D.A. Coyle, J. Duyster, F. Henjes-Kunst, A. Peterek, B. Schröder, B. Stöckhert, K. Wemmer, G. Zulauf, H. Ahrendt, R. Bischoff, E. Hejl, J. Jacobs, D. Menzel, N. Lal, P. Van den haute, C. Vercoutere, B. Welzel, Post-Variscan thermal and tectonic evolution of the KTB site and its surroundings, J. Geophys. Res. 102 (B8) (1997) 18221–18232.

[8] D.A. Coyle, G.A. Wagner, Fission-track investigations on sphene from KTB Deep Drilling Project (Germany): post-Permian cooling history and in situ annealing, KTB Report 94-2, 1994, pp. 63–70.

[9] F. Henjes-Kunst, A. Höhndorf, H. Kreuzer, E. Seidel, K/Ar and Ar/Ar dating on minerals of the KTB, KTB Report 94-2, 1994, B33.

[10] K. Wemmer, H. Ahrendt, Age determinations on retrograde processes and investigations on the blocking conditions of isotope systems of KTB rocks, KTB Report 94-2, 1994, B32.

[11] W. Franke, The geological framework of the KTB drill site, Oberpfalz, in: R. Emmerman, J. Wohlenberg (Eds.), The German Continental Deep Drilling Program (KTB), Springer-Verlag, New York, 1989, pp. 37–54.

[12] C. Reichert, H.-J. Dürbaum, G. Hirschmann, P. Sadowiak, H. Wiederhold, M. Stiller and DEKORP Research Group, Thickness and signature estimation of the SE1 seismic event at the KTB Oberpfalz, KTB Report 93-2, 1993, pp. 137–139.

[13] J. Duyster, A. Grawinkel, A. Kontny, Petrographic and structural characterization, KTB Report 95-2, 1995, B1–B80.

[14] G. Hirschmann, Das Bruchstörungsmuster im KTB-Umfeld, KTB Report 92-3, 1992, pp. 85–124.

[15] B. Schröder, Inversion tectonics along the western margin of the Bohemian Massif, Tectonophysics 137 (1987) 93–100.

[16] B. Schröder, H. Ahrendt, A. Peterek, K. Wemmer, Post-Variscan sedimentary record of the SW margin of the Bohemian massif: a review, Geol. Rundsch. 86 (1997) 178–184.

[17] V. Sibrava, P. Havlicek, Radiometric age of Plio–Pleistocene volcanic rocks of Bohemian Massif, Bull. Geol. Surv. Prague 55 (1980) 129–140.

[18] T. Kohl, L. Rybach, Thermal and hydraulic aspects of the KTB drill site, Geophys. J. Int. 124 (1996) 756–77219.

[19] M. Kastner, Authigenic feldspars in carbonate rocks, Am. Mineral. 56 (1971) 1403–1442.

[20] M. Kastner, R. Siever, Low temperature feldspars in sedimentary rocks, Am. J. Sci. 279 (1979) 435–479.

[21] I. McDougall, Z. Roksandic, Total fusion 40Ar/39Ar ages using HIFAR reactor, Geol. Soc. Aust. J. 21 (1974) 81–89.

[22] Th. Staudacher, E.K. Jessberger, D. Dörflinger, J. Kiko, A refined ultrahigh-vacuum furnace for rare gas analysis, J. Phys. E Sci. Instrum. 11 (1978) 781–784.

[23] R.H. Steiger, E. Jäger, Convention on the use of decay constants in geo- and cosmochronology, Earth Planet. Sci. Lett. 36 (1977) 359–362.

[24] T.M. Harrison, M.T. Heizler, O.M. Lovera, In vacuo crushing experiments and K-feldspar thermochronometry, Earth Planet. Sci. Lett. 117 (1993) 169–180.

[25] P.K. Zeitler, Inversion of $^{40}Ar/^{39}Ar$ age spectra using the controlled-random-search method, EOS Trans. Am. Geophys. Union 74 (1993) 650.

[26] O.M. Lovera, M. Grove, T.M. Harrison, M.T. Heizler, Systematic analysis of K-feldspar age and kinetic properties, EOS Trans. Am. Geophys. Union 76 (1995) 287.

[27] O.M. Lovera, F.M. Richter, T.M. Harrison, The $^{40}Ar/^{39}Ar$ thermochronology for slowly cooled samples having a distribution of diffusion domain sizes, J. Geophys. Res. 94 (1989) 17917–17931.

[28] T.M. Harrison, I. McDougall, Excess ^{40}Ar in metamorphic rocks from Broken Hill, New South Wales: implications for $^{40}Ar/^{39}Ar$ age spectra and the thermal history of the region, Earth Planet. Sci. Lett. 55 (1981) 123–149.

[29] P.K. Zeitler, J.D. Fitz Gerald, Saddle shaped $^{40}Ar/^{39}Ar$ age spectra from young microstructurally complex potassium feldspars, Geochim. Cosmochim. Acta 50 (1986) 1185–1199.

[30] O.M. Lovera, F.M. Richter, T.M. Harrison, Diffusion domains determined by ^{39}Ar released during step heating, J. Geophys. Res. 96 (1991) 2057–2070.

[31] F.M. Richter, O.M. Lovera, T.M. Harrison, Tibetan tectonics from $^{40}Ar/^{39}Ar$ analysis of a single feldspar sample, Earth Planet. Sci. Lett. 105 (1991) 266–278.

[32] D.A. Foster, T.M. Harrison, P. Copeland, M.T. Heizler, Effects of excess argon within large diffusion domains on

K-feldspar age spectra, Geochim. Cosmochim. Acta 54 (1990) 1699–1708.

[33] P. Möller, S. Weise, E. Althaus, W. Bach, H. Behr, R. Borchardt, K. Bräuer, J. Drescher, J. Erzinger, E. Faber, B. Hansen, E. Horn, E. Huenges, H. Kämpf, W. Kessels, T. Kirsten, D. Landwehr, M. Lodemann, L. Machon, A. Pekdeger, H. Pielow, C. Reutel, K. Simon, J. Walther, F. Weinlich, M. Zimmer, Paleofluids and recent fluids in the upper continental crust: results from the German Continental Deep Drilling Program (KTB), J. Geophys. Res. 102 (B8) (1997) 18233–18254.